JOURNAL OF MECHANICAL ENGINEERING AND SCIENCES
ISSN: 2289-4659 e-ISSN: 2231-8380
VOLUME 19, ISSUE 4, 2025, 10985 - 10997
DOI: https://doi.org/10.15282/jmes.19.4.2025.11.0859

RESEARCH ARTICLE

Heat transfer characteristics of a battery liquid-cooling system based on inverted T-shaped oscillating heat pipe with nanofluids

L. Hongkun[1,2], M. M. Noor[1,3]*, K. Kadirgama[1], M. S. Beg[1]

[1] Faculty of Mechanical and Automotive Engineering Technology, Universiti Malaysia Pahang Al-Sultan Abdullah, 26600 Pekan, Pahang, Malaysia
[2] School of Automotive Engineering, Jiangxi Polytechnic University, Jiujiang 332000, Jiangxi, China
[3] Centre for Research in Advanced Fluid and Processes, Universiti Malaysia Pahang Al-Sultan Abdullah, 26600 Pekan, Pahang, Malaysia

ABSTRACT - Developing efficient and reliable battery thermal management systems (BTMS) has emerged as a key focus in EV research. The oscillating heat pipe (OHP) is a relatively new technology in BTMS applications. This study proposes a novel hybrid BTMS based on an inverted T-shaped OHP to enhance the heat transfer performance through the coupling of liquid cooling with OHP cooling. Equivalent thermal resistance experiments were used to comprehensively analyze the effect of graphene nanofluid coolant on the hybrid BTMS. The results indicate that increasing the concentration of graphene nanofluids further improves the cooling performance of the hybrid BTMS. At 280W with a concentration of 0.2 wt%, the equivalent BTMS thermal resistance (R_{BTMS}) and maximum temperature (T_{max}) are reduced by 20.2% and 32.9%, respectively. However, increasing nanofluid concentration weakens the forced convection effect of the working fluid between the evaporation and condensation sections of the OHP, thereby decreasing the OHP's heat transfer performance within the BTMS. This study deepens the comprehension of the performance enhancement effects of nanofluid coolant in the hybrid system, providing practical guidance for OHP-based cooling system development.

ARTICLE HISTORY
Received : 16th Oct. 2024
Revised : 09th Oct. 2025
Accepted : 12th Oct. 2025
Published : 29th Dec. 2025

KEYWORDS
Oscillating heat pipe
Battery thermal management system
Graphene nanofluid coolant
Heat transfer characteristics
Liquid cooling

1. INTRODUCTION

Currently, lithium-ion batteries are the primary power source for electric vehicles (EVs), but considerable heat is generated during high-power charging and discharging cycles [1]. Ineffective dissipation of this heat can cause performance degradation, reduced lifespan, and thermal runaway, presenting serious safety concerns [2-4]. Therefore, the development of efficient and reliable battery thermal management systems (BTMS) is crucial for advancing EV technology [5-7]. Existing battery cooling technologies include air cooling [8, 9], liquid cooling [10, 11], phase change material (PCM) cooling [12, 13], and heat pipe cooling [14-16]. Among these, the oscillating heat pipe (OHP) presents a promising BTMS solution due to its high heat transfer efficiency, simple structure, and lightweight design [17]. Unlike other methods, the OHP relies on the oscillatory motion of vapor and liquid plugs, driven by pressure imbalances, to achieve efficient heat transfer without the need for additional mechanical work. Its strong environmental adaptability also ensures stable operation under varying conditions [18]. Applying the OHP in BTMS can significantly reduce the average battery temperature and improve temperature uniformity, thereby extending battery life and enhancing EV performance [19].

The geometry of an OHP significantly influences its performance [20]. Given the diverse structures of OHPs, they can be flexibly designed to match the specific characteristics of the system they are intended to cool. When applied to battery thermal management systems, OHPs must be tailored to the structure of the battery or battery pack being studied [21]. Figure 1 depicts various OHP structures utilized in battery thermal management systems in recent years. The flexibility of OHPs, which enables them to be readily bent and shaped, allows for the design of suitable OHP structures tailored to different battery types, such as pouch cells, prismatic batteries, and cylindrical batteries. It is important to note that the majority of current research on the application of OHPs in battery thermal management systems concentrates on verifying the OHP's capacity to dissipate heat or offer thermal insulation for batteries [22, 23]. Consequently, the most prevalent structure, as depicted in Figure 1a, is the 2D planar OHP. In the design of such systems, it is crucial to ensure that the evaporator section of the OHP corresponds with the dimensions of the corresponding prismatic battery and that the condenser section is compatible with the cooling system [24]. Additionally, as shown in Figure 1b, a tube-plate structure can be used, where the evaporator section of the OHP is embedded within a slotted heat-collecting plate [25]. This design increases the contact area between the OHP's evaporator section and the battery surface, thereby reducing contact thermal resistance and enhancing heat transfer efficiency. As research into the application of OHPs in battery thermal management systems advances, innovative structural designs continue to emerge. For example, Chotmanee et al. introduced a check valve into the OHP, as depicted in Figure 1c, which led to a lower start-up temperature and reduced start-up time. In a closed-loop OHP equipped with a check valve, the maximum heat transfer achieved was 98.6 W, which decreased the simulated battery temperature to 55.8°C [26]. As shown in Figure 1d, Lv et al. conducted research on the

*CORRESPONDING AUTHOR | M. M. Noor | ✉ muhamad@umpsa.edu.my

thermal management of battery modules using multiple 2D OHPs [27]. In another innovation, as shown in Figure 1e, Chi et al. modified the traditional U-shaped bends at the bottom of the OHP to a right-angle design, further reducing the vertical length of the condenser section [28]. This modification is beneficial for improving space utilization within a vehicle. Similarly, as depicted in Figure 1f, Chi et al. proposed an L-shaped OHP characterized by a longer heating section and shorter cooling and adiabatic sections. This design facilitates a more compact spatial arrangement between the battery and the cooling system [29]. For cylindrical batteries, the OHP structures are typically more complex, as seen in Figure 1g and Figure 1h [30, 31], to maximize the contact area between the OHP and the battery. Consequently, research on BTMS based on OHP should begin with structural innovations that enhance both the volumetric efficiency of the battery system and its heat transfer performance.

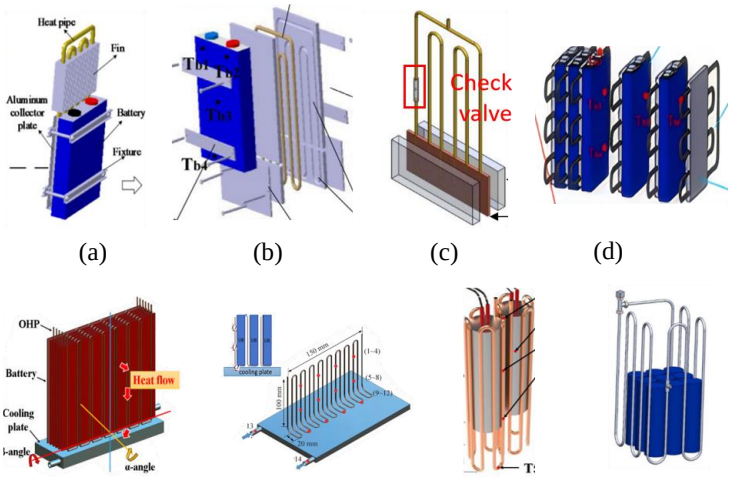

(a) (b) (c) (d)

(e) (f) (g) (h)

Figure 1. Various OHP structures for BTMS

To achieve superior cooling performance and reduce temperature gradients, the authors propose a novel system that integrates a vertically oriented OHP with a liquid cooling plate, as shown in Figure 2. This system utilizes the vertical design of the inverted T-shaped OHP, which is especially well-suited to the structural characteristics of prismatic batteries. Unlike conventional liquid cooling plates, this innovative cooling system integrates the condenser section of the OHP into the center of the liquid cooling plate. This configuration ensures direct contact between the cooling plate's surface and the battery cells, facilitating effective heat dissipation without the requirement for additional cooling devices. Moreover, the system efficiently utilizes the OHP for enhanced heat transfer. The study delves deeper into the impact of graphene nanofluids as a coolant on the thermal performance of the proposed hybrid BTMS, highlighting the potential of nanofluids to enhance the heat transfer capabilities of this innovative design.

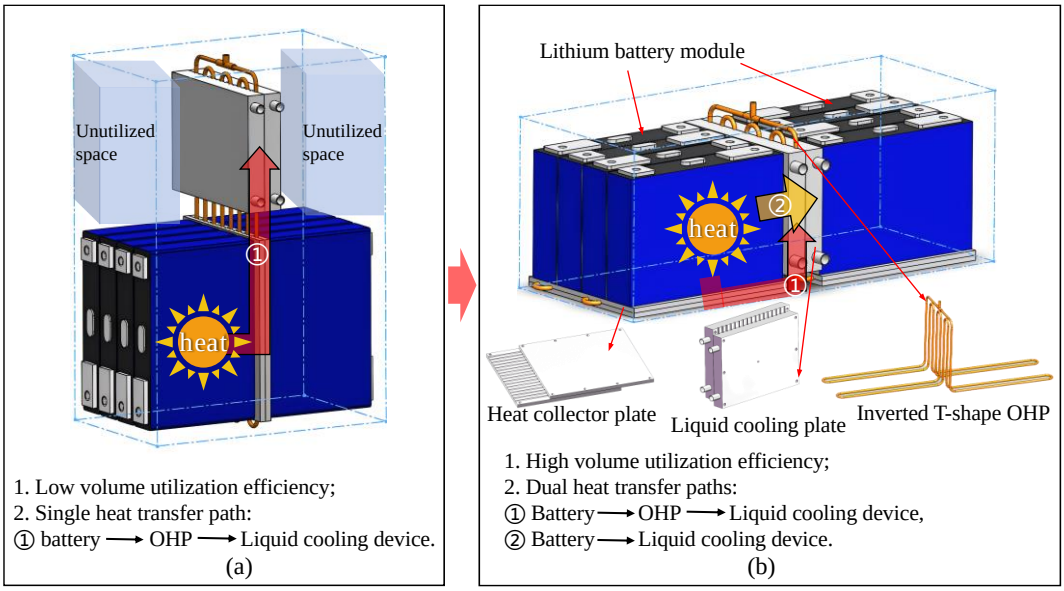

Figure 2. Schematic of the hybrid BTMS

2. MATERIALS AND METHODS

2.1 Experimental System Design

To investigate the performance of the proposed cooling system, an experimental setup was designed and constructed, as depicted in Figure 3. The experimental system mainly comprises a simulated battery module (serving as the heat source), an inverted T-shaped OHP, a heat-collecting plate, a liquid cooling plate, a water-cooling unit, a heat dissipation system, and a data acquisition system. To minimize heat loss from the experimental system to the surrounding environment, aluminum foil and insulation cotton were utilized for thermal insulation. Thermally conductive silicone pads were positioned between the heat-collecting plate, the liquid cooling plate, and the simulated battery to reduce contact thermal resistance. The design of the experimental rig aligns with the team's previous work on studying the effects of pulsating flow on the performance of BTMS based on an inverted T-shaped OHP. Detailed experimental design and procedures are available in reference [32]. The uncertainties and accuracies of the instruments used in the experiment are detailed in Table 1.

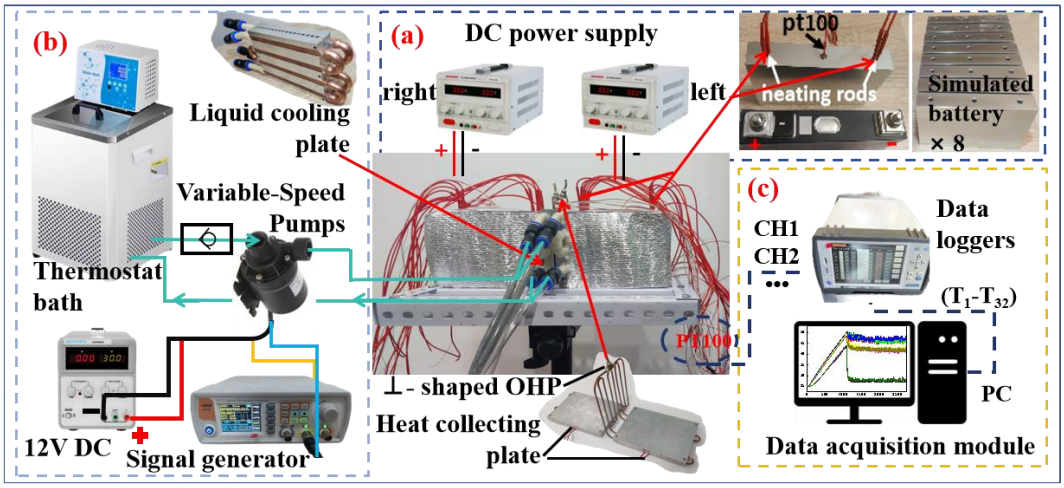

Figure 3. Test bench schematic

Table 1. Instrument accuracy and uncertainty

Parameters	Type	Accuracy	Uncertainty
Temperature sensor (℃)	PT-100	0.1%	±0.1 ℃
Temperature logger (℃)	ZC300V-64	0.1%	±0.1 ℃
DC power supply (V)	MS10030D	0.1%	±0.005 V
Variable-speed pump (L/min)	TL-B10H	0.2%	±0.02 L/min
Thermostatic bath (℃)	HX-101	0.05%	±0.05 ℃

It is noteworthy that this study utilized aluminum blocks with the same dimensions as the LP-51Ah ternary prismatic lithium-ion battery. Electric heating rods were placed at the positions corresponding to the positive and negative electrodes to simulate the battery heating process. This configuration facilitates the analysis of the effects on the battery's thermal management system. Additionally, a hole was drilled at the center of each cell to accommodate the installation of a PT100 temperature sensor (refer to Figure 3.a), allowing for real-time monitoring and recording of temperature fluctuations in the core area.

While heating blocks have limitations in replicating the dynamic heat generation characteristics of actual batteries, they can still serve as a reliable benchmark. This setup allows for the evaluation of the heat load applied to the heating blocks during experiments and enables a quantitative analysis of the cooling performance advantages of the hybrid system over conventional liquid cooling systems. According to the technical manual, the battery is rated for a peak discharge of 3C. The equivalent heat loads for the 8 cells at discharge rates of 1C, 2C, and 3C were 30W, 47W, and 90W, respectively, with the peak load reaching 277.6W.

2.2 OHP Design and Processing

The structural parameters of an OHP have a significant impact on its performance. In this study, the OHP is specifically designed for battery thermal management, ensuring that the battery surface temperature does not exceed 60°C. Therefore, it is essential to design and fabricate an OHP with exceptional start-up performance to guarantee its effective operation. The startup performance is closely related to physical properties such as the saturation pressure gradient $(dP/dT)_{sat}$, surface tension, and viscosity [33]. Consequently, acetone, which exhibits a higher $(dP/dT)_{sat}$ value, was chosen as the working fluid, and a relatively low filling ratio was utilized. The specific parameters of the OHP used in the experiments are detailed in Table 2.

Table 2. Key dimensional parameters of the OHP

Variables	Parameters
Material	Brass
Inner Diameter (mm)	2
Outer Diameter (mm)	3
Working fluid	acetone
Filling rate	26.1%
Evaporation Section Length (mm)	148
Adiabatic Section Length (mm)	25
Condensation Section Length (mm)	100
Number of Bends	4
Bend Radius (mm)	7

2.3 Data Collection and Processing

Given the inherent randomness in the movement of the working fluid within an OHP, it is essential to account for temperature variations at different locations when distributing PT100 temperature sensors. The distribution of temperature measurement points on the OHP is depicted in Figure 4. Points T1–T4 are located in the evaporator section, T5–T8 in the adiabatic section, and T9–T12 in the condenser section. Additionally, the surface temperatures of the No. 1, No. 3, No. 6, and No. 8 simulated batteries were monitored, with identical temperature measurement points for each battery. As shown in Figure 4.b, using the No. 1 simulated battery as an example, T15 is a probe-type PT100 sensor used to measure the central temperature of the battery (refer to Figure 3.a). T13 and T14 measure temperatures near the heat-collecting plate, while T16 and T17 measure temperatures farther from the heat-collecting plate. T13 and T16 are positioned closer to the liquid cooling plate.

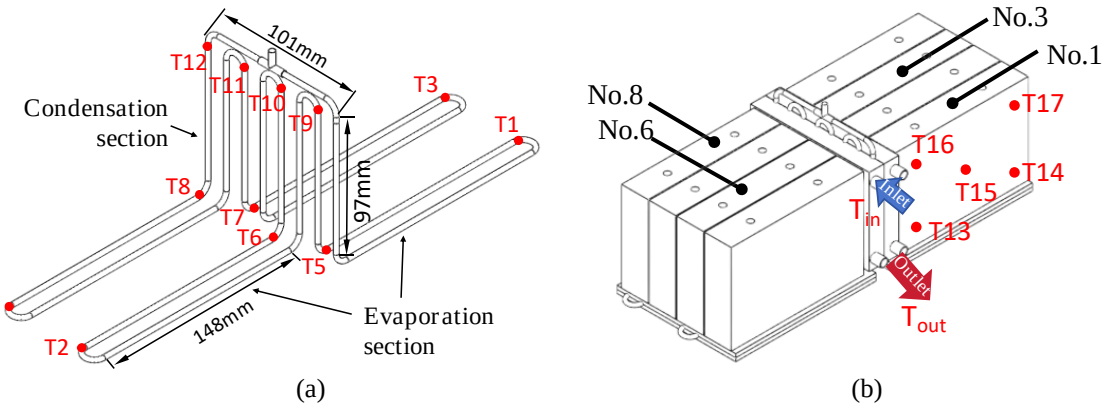

Figure 4. Layout of temperature measuring points: (a) the points on the OHP, (b) the points on the No. 1 battery

The key performance indicators for an OHP include thermal resistance, the temperature difference between the evaporator and condenser sections, and the temperature uniformity within the evaporator section. Thermal resistance is defined by Eq. (1).

$$R = \frac{T_{eva} - T_{con}}{Q_{OHP}} \tag{1}$$

$$T_{eva} = \frac{1}{n_1}\sum_{i=1}^{n_1} Ti \tag{2}$$

$$T_{eva} = \frac{1}{n_1}\sum_{i=1}^{n_1} Ti \tag{3}$$

In the equation, T_{eva} and T_{con} represent the average wall temperatures of the evaporator and condenser sections, respectively. Q_{OHP} denotes the heat transfer rate of the OHP. The terms n_1 and n_2 correspond to the number of temperature measurement points arranged in the evaporator and condenser sections, respectively. The unit of thermal resistance is °C/W.

The cooling performance of a BTMS can be directly assessed by the temperature and temperature difference within the battery pack. Improved cooling performance leads to lower maximum and average surface temperatures of the battery, as well as a reduced temperature difference. Therefore, this study primarily focuses on the average battery temperature

(T_b), the maximum temperature (T_{max}), the maximum temperature difference (ΔT_{max}), and the equivalent BTMS thermal resistance (R_{BTMS}). Their definitions are as follows:

$$T_b = \frac{1}{n}\sum_{i=1}^{n} Ti \tag{4}$$

$$T_{max} = max\{T1, T2, \ldots Ti, \ldots Tn\} \tag{5}$$

$$\Delta T_{max} = T_{max} - T_{min} \tag{6}$$

$$R_{BTMS} = \frac{T_b - T_{out}}{Q_{total}} \tag{7}$$

In these definitions, n represents the number of temperature measurement points within the battery pack, Ti denotes the battery surface temperature at the i-th measurement point, and T_{out} refers to the outlet temperature of the coolant.

2.4 Preparation of graphene nanofluids

As depicted in Figure 5, the graphene nanoparticles utilized in this experiment were custom-manufactured by Chengdu Jiacai Technology Co., Ltd. These nanoparticles are composed of few-layer, sheet-like graphene with an average thickness not exceeding 3 nm and an average diameter ranging from 0.5 to 3 μm. The thermal conductivity is 3300 W/(m·K), and the specific surface area falls between 500 and 800 m²/g [34].

Figure 5. Few-layered graphene particles

The color and surface wrinkles in scanning electron microscope (SEM) images can provide a rough estimate of the number of graphene layers. Figure 6 shows the SEM images of the graphene used in this study. The images reveal the typical flake-like layered structure of graphene. As the graphene was prepared using the Hummers method, it features relatively thin layers with distinct, wave-like wrinkles along the edges of the sheets [35].

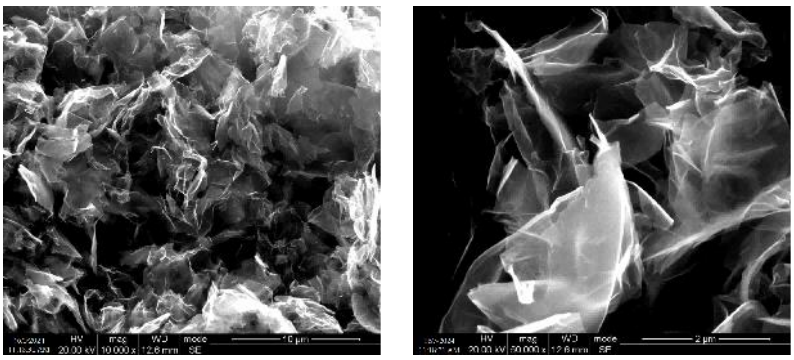

Figure 6. SEM photo of graphene

To enhance the dispersibility and stability of graphene nanoparticles in solution, polyvinylpyrrolidone (PVP) was selected as the dispersant, and a two-step method was used to prepare the nanofluid [36]. Initially, a base fluid was prepared by mixing PVP with pure water at a mass ratio of 1.5:98.5. Subsequently, graphene nanoparticles were introduced into the base fluid and stirred at room temperature using a magnetic stirrer for 20 minutes. The mixture was then subjected to ultrasonic treatment in a sonicator, vibrating the solution three times for 30 minutes each session. Based on experimental requirements, graphene nanofluid suspensions with mass fractions ranging from 0.05% to 0.2% were prepared. The stability of graphene nanofluids is crucial for their performance parameters. As depicted in Figure 7, the stability of the graphene nanofluids was evaluated using a simple and convenient visual sedimentation method. After allowing samples of various graphene nanofluids concentrations to remain undisturbed for 48 hours, no significant sedimentation was observed, indicating that the graphene nanofluids exhibited good stability.

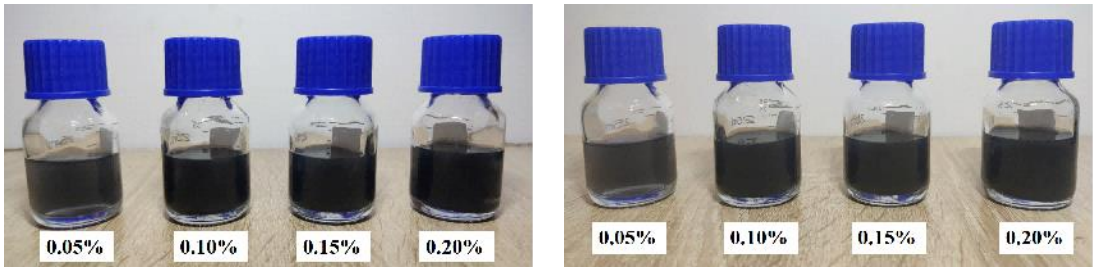

(a) (b)

Figure 7. Photographs of graphene nanofluids samples with varying concentrations: (a) just prepared, and (b) after a 48-hour period

2.5 Experimental Plan

As shown in Figure 8, this study examines the enhanced heat transfer characteristics of the hybrid BTMS using nanofluids, with a conventional liquid BTMS serving as the control group.

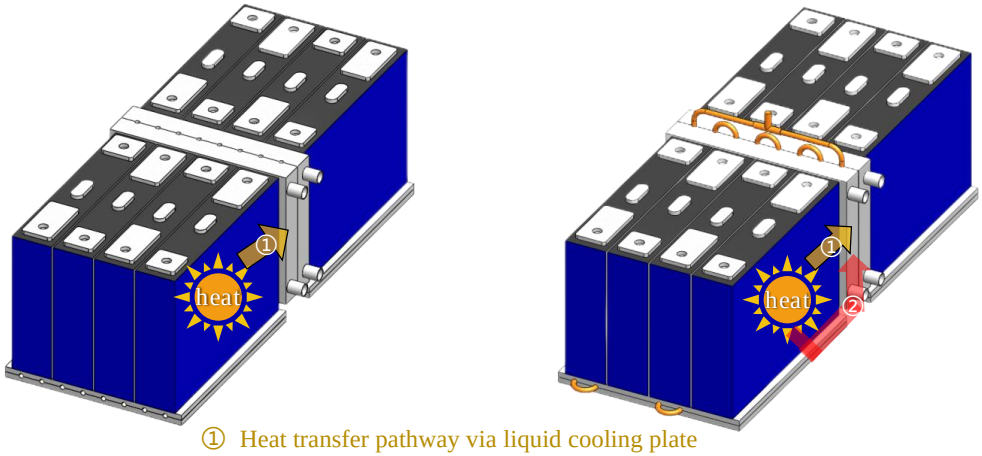

(a) (b)

Figure 8. Different BTMS: (a) liquid BTMS (control group), (b) hybrid BTMS

This study primarily investigates the impact of graphene nanofluid coolants at different concentrations on the performance of the hybrid BTMS. The experimental conditions for this study are detailed in Table 3.

Table 3. The main experimental conditions

Variables	Parameter
BTMS system	liquid BTMS, hybrid BTMS
Heating load /(W)	200, 220, 240, 260, 280, 300
Coolant temperature / (℃)	25
Cooling starting temperature / (℃)	45
Flow type	Constant flow
Flow rate /(L/min)	2.6
Nanofluids /(wt%)	0%, 0.05%, 0.1%, 0.15%, 0.2%

It is important to note that in the composite cooling system presented in this study, the heat generated by the battery can be dissipated either directly through the liquid cooling plate or via the OHP. Therefore, the new system incorporates two distinct heat dissipation pathways. Due to this dual-path configuration, it is not possible to directly measure the amount of heat (Q_{OHP}) removed by the OHP. Instead, the performance of the OHP is primarily assessed through the wall temperature of the evaporator section and the oscillation patterns of the working fluid. The overall performance of the battery cooling system can be evaluated by analyzing T_b, T_{max}, ΔT_{max}, and the R_{BTMS}.

2.6 Error Analysis

During the experiments, the primary sources of error include direct measurement errors and indirect measurement errors. This study focuses on a battery liquid cooling system based on an inverted T-shaped OHP, with particular emphasis on the temperature data collected from the battery pack and various temperature measurement points on the OHP. The errors can be calculated using the law of error propagation [27]. Table 4 lists the main parameters and their associated errors involved in this chapter's experiments.

Table 4. Experimental uncertainties of main parameters

Parameters	Uncertainty (%)
Ti (i=1,2----32)	±1.0%
T_{max}	±1.0%
Q	0.4%
R	3.8%

3. RESULTS AND DISCUSSION

As shown in Figure 9, the thermal conductivity and viscosity of graphene nanofluid coolants with different mass fractions were measured at ambient temperature (25℃). When the mass fraction is 0, the coolant is deionized water. The figure shows that the addition of graphene nanofluids increases both the thermal conductivity and viscosity of the coolant [37]. Moreover, as the concentration of the nanofluid increases, the thermal conductivity shows a more significant rise. Compared to deionized water, when using a graphene nanofluids with a mass fraction of 0.2%, the thermal conductivity increases from 0.603 W/(m·K) to 1.06 W/(m·K), and the viscosity increases from 0.865×10^{-3} Pa·s to 1.09×10^{-3} Pa·s. This represents an increase of 75.8% in thermal conductivity and 26.0% in viscosity. Obviously, as a nanofluid additive, graphene can significantly enhance the thermal conductivity and heat transfer efficiency of coolants, demonstrating significant application potential [38]. These findings demonstrate that while graphene nanofluids significantly improve the heat conduction properties of the coolant, they also introduce a certain level of increased flow resistance. However, the hybrid BTMS investigated in this study combines both liquid cooling and inverted T-shaped OHP systems, and the comprehensive effects of nanofluids on this composite system remain unclear. Therefore, this project applies graphene nanofluid as the coolant to experimentally study its heat transfer enhancement effects on the hybrid BTMS.

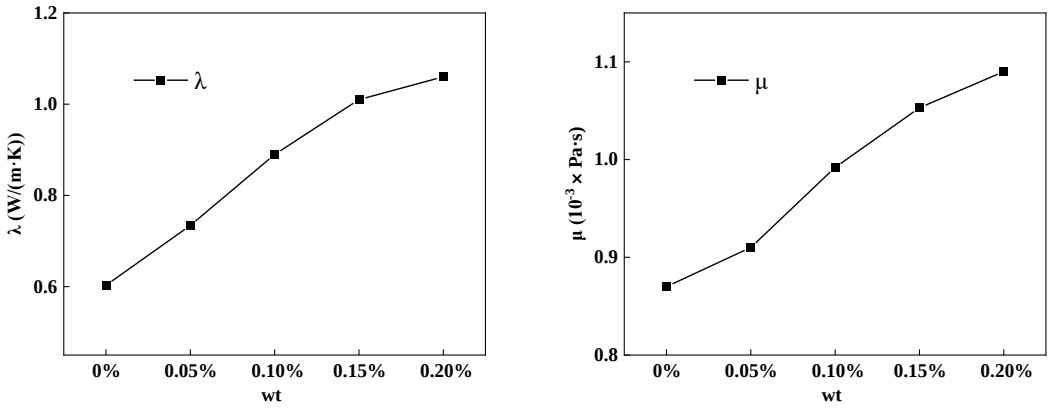

(a) (b)

Figure 9. Physical properties of nanofluids at different concentrations: (a) thermal conductivity, (b) viscosity

To investigate the enhancement effect of nanofluids on the heat transfer performance of the hybrid BTMS, Figure 10 illustrates the variation in the average battery temperature (T_b) with heat load for graphene nanofluids with mass concentrations of 0.05%, 0.1%, 0.15%, and 0.2%. Increasing the concentration of graphene nanofluids improves their thermal conductivity, thereby enhancing the heat transfer efficiency of the hybrid BTMS [39]. Overall, under the same heat load, the T_b of the hybrid BTMS is lower when using graphene nanofluid coolant compared to regular coolant. Additionally, as the graphene nanofluids concentration increases, the T_b value decreases. For example, under a heat load of 260W, the T_b value is 49.1°C with water coolant, while it drops to 47.8°C, 47.2°C, 46.8°C, and 46.6°C with graphene nanofluids concentrations of 0.05%, 0.1%, 0.15%, and 0.2%, respectively. This indicates that as the concentration of graphene nanofluids increases, the incremental benefits of higher concentrations on the hybrid BTMS diminish. This phenomenon can be attributed to two main factors. First, once the concentration of graphene nanofluids reaches a certain threshold, further increases in concentration have a limited effect on improving the thermal conductivity of the coolant. Second, the nanofluids significantly enhance the liquid cooling efficiency within the hybrid BTMS. As the total heat load remains constant, this reduces the heat load on the inverted T-shaped OHP, thereby diminishing the heat transfer efficiency of the OHP.

At 200-240W, the T_b is actually higher when using a 0.05% mass fraction nanofluid compared to water coolant. For instance, at 200W, the T_b value is 44.3° C with water coolant, but it rises to 44.5° C when using the 0.05 wt% nanofluid. This occurs because, in the 200-240W heat load range, the inverted T-shaped OHP in the hybrid BTMS operates stably with water as the coolant. In contrast, when nanofluid coolant is used, the inverted T-shaped OHP cannot operate stably and eventually fails. The enhancement in cooling performance provided by the 0.05 wt% nanofluid is smaller than the improvement gained from the stable operation of the inverted T-shaped OHP. However, once the heat load increases to 260W, the inverted T-shaped OHP with nanofluid as the coolant can stabilize, enabling the dual heat transfer pathways

of the hybrid BTMS to function effectively. Interestingly, despite the increase in heat load to 260W, the T_b value decreases or remains almost unchanged at the same concentration of graphene nanofluid compared to 240W.

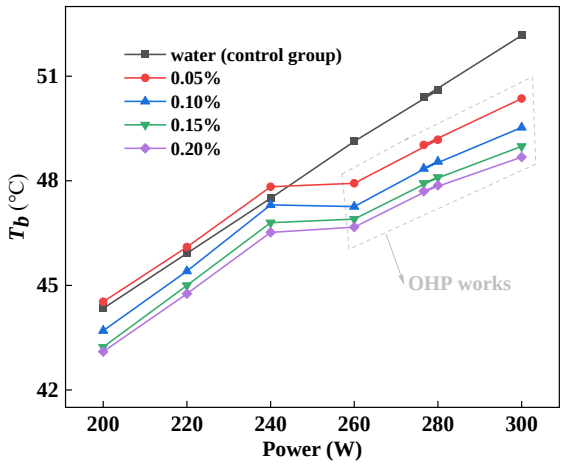

Figure 10. T_b of the battery pack in the hybrid BTMS with different concentrations of nanofluid coolant

As shown in Figure 11, the oscillating temperature curves of the evaporator section of the inverted T-shaped OHP and the corresponding rate of temperature change per second under different graphene nanofluids concentrations at 280W are presented. Overall, similar to the trend observed in the battery pack's T_b in the hybrid BTMS, the average oscillating temperature in the evaporator section decreases as the concentration of graphene nanofluids increases. When pure water is used as the coolant, the evaporator section operates with an oscillating temperature around 46.8°C. However, with graphene nanofluids concentrations of 0.05%, 0.1%, 0.15%, and 0.2%, the average oscillating temperatures in the evaporator section drop to 44.7°C, 44.3°C, 43.8°C, and 43.7°C, respectively. It is noteworthy that as the temperature of the evaporator section in the OHP decreases, the temperature difference between the evaporator and condenser sections also declines, resulting in a reduced driving force within the heat pipe. From the temperature oscillation curves, the amplitude of temperature oscillation is largest when pure water is used as the coolant, with no apparent stagnation in the oscillation. However, as the concentration of graphene nanofluids increases, the amplitude of temperature oscillation in the evaporator section decreases. At concentrations of 0.15% and 0.2%, there are periods where the temperature in the evaporator section experiences oscillation stagnation, indicating that the oscillatory motion of the working fluid weakens, transitioning the heat pipe from large to small amplitude oscillations. This trend is also clearly reflected in the rate of temperature change per second, where the magnitude of the rate decreases as the concentration of graphene nanofluids increases. Additionally, the frequency of temperature changes also declines, suggesting that under constant heat load, the forced convection effect between the evaporator and condenser sections weakens as the graphene nanofluids concentration rises. This reduction in forced convection consequently decreases the heat transfer performance of the OHP.

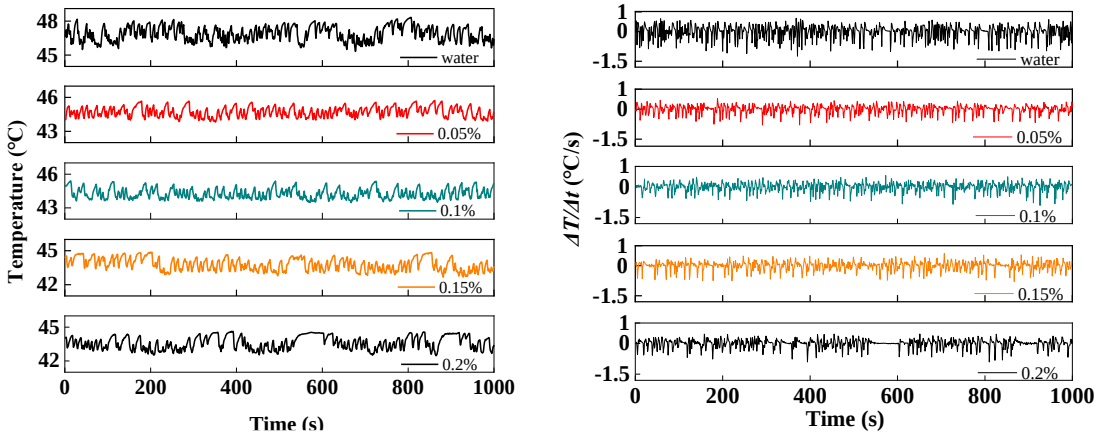

(a) (b)

Figure 11. Temperature fluctuations of OHP in the hybrid BTMS with different concentrations of nanofluid coolant under 280W: (a) temperature oscillation curves, (b) temperature change rate curves

Table 5 presents the steady-state temperature values at each measurement point in the BTMS under an equivalent heat load of 3C heat release ratio (280W), using water as the coolant in both the hybrid BTMS and the liquid BTMS. T1-T12 are temperature measurement points on the OHP wall. T1–T4 are located in the evaporator section, T5–T8 in the adiabatic section, and T9–T12 in the condenser section. It is worth noting that there is no OHP in the liquid BTMS. T13-T17, T18-T22, T23-T27, and T28-T32 correspond to the surface temperature measurement points of four battery groups. Overall, in both systems, the closer the temperature measurement point is to the

cooling plate, the lower the temperature. The highest temperature in each battery group is located at the point farthest from both the cooling plate and the evaporator section of the OHP, which are T17, T22, T27, and T32. Among all the measurement points, T32, located under No. 8 battery, has the highest temperature. As the working medium in the OHP oscillates stably, heat transfer occurs between the evaporation and condensation sections. Taking the evaporation section (T1 – T4) as an example, the wall oscillation temperature is stabilized within the range of 43℃ to 44℃. The stable operation of the OHP provides additional heat transfer path, the hybrid BTMS demonstrates significantly better cooling performance than the liquid BTMS. Specifically, the temperature at points farther from the cooling plate in the hybrid BTMS (T14, T17, T19, T22, T24, T27, T29, T32) is approximately 3.2°C lower than in the liquid BTMS. Ultimately, the T_b, T_{max}, and ΔT_{max} values in the hybrid BTMS are 50.6°C, 52.8°C, and 4.1°C, respectively. Compared to the liquid BTMS, the hybrid BTMS reduces T_b, T_{max}, and ΔT_{max} by 2.6°C, 3.2°C, and 1.0°C, respectively. This proves that, by integrating the OHP and the liquid cooling plate in a "parallel" heat transfer configuration, the system effectively increases the heat transfer interface area, thereby reducing the overall thermal resistance and improving the temperature uniformity of the battery pack significantly.

Table 5. Temperatures at each point of the battery pack under different BTMS with water coolant (280W)

BTMS types	Temperature points of the inverted T-shaped OHP and battery pack (°C)							
	T1	T2	T3	T4	T5	T6	T7	T8
liquid BTMS	/	/	/	/	/	/	/	/
Hybrid BTMS	45.1–48.1	45.2–47.9	45.0–48.2	44.8–47.9	41.0–43.1	40.6–42.9	41.2–43.3	40.8–43.1
	T9	T10	T11	T12	T13	T14	T15	T16
liquid BTMS	/	/	/	/	51.3	54.7	52.9	50.8
Hybrid BTMS	27.0–28.3	27.3–29.0	27.4–28.8	27.1–28.5	49.7	50.9	50.2	48.9
	T17	T18	T19	T20	T21	T22	T23	T24
liquid BTMS	55.1	51.2	55.1	53.3	50.9	55.3	51.3	55.2
Hybrid BTMS	51.9	49.6	51.5	50.4	48.9	52.4	49.8	51.8
	T25	T26	T27	T28	T29	T30	T31	T32
liquid BTMS	53.5	50.9	55.6	51.3	55.6	53.7	50.8	56.0
Hybrid BTMS	50.6	49.1	52.7	49.9	51.9	50.6	49.0	52.8

Table 6. Temperatures at each point of the battery pack under different BTMS with nanofluid coolant (280W)

BTMS types	Temperature points of the inverted T-shaped OHP and battery pack (°C)							
	T1	T2	T3	T4	T5	T6	T7	T8
liquid BTMS	/	/	/	/	/	/	/	/
Hybrid BTMS	42.5–44.6	42.7–44.9	42.4–44.5	42.5–44.7	38.9–40.5	39.0–40.7	38.9–40.6	38.8–40.5
	T9	T10	T11	T12	T13	T14	T15	T16
liquid BTMS	/	/	/	/	48.1	50.7	49.2	47.7
Hybrid BTMS	26.8–28.0	26.9–28.3	26.8–28.1	26.7–28.3	47.1	48.3	47.6	46.3
	T17	T18	T19	T20	T21	T22	T23	T24
liquid BTMS	51.0	48.3	50.9	49.7	47.9	51.1	48.3	51.0
Hybrid BTMS	49.0	47.0	48.5	47.9	46.2	49.3	47.1	48.8
	T25	T26	T27	T28	T29	T30	T31	T32
liquid BTMS	49.9	47.9	51.3	48.4	51.2	50.1	48.1	51.5
Hybrid BTMS	48.2	46.4	49.5	47.3	49.1	48.5	46.4	49.8

Table 6 presents the steady-state temperature values at various measurement points in the BTMS under 280W, using a 0.2% mass concentration graphene nanofluids as the coolant in both the hybrid BTMS and the liquid BTMS. Overall, with the nanofluid, the inverted T-shaped OHP operates stably at a 280W load, making the heat transfer pathway of the oscillating heat pipe in the hybrid BTMS effective. As a result, the hybrid BTMS, which benefits from a dual heat transfer pathway, exhibits superior heat transfer performance compared to the liquid BTMS, with lower steady-state temperature values at all measurement points on the battery pack. The highest temperatures in the battery pack occur at the points farthest from both the cooling plate and the evaporator section of the oscillating heat pipe, specifically at T17, T22, T27, and T32. In the hybrid BTMS, the temperature values at T17, T22, T27, and T32 are 49.9°C, 49.3°C, 49.5°C, and 49.8°C. In contrast, the corresponding temperatures in the liquid BTMS are 51.0°C, 51.1°C, 51.3°C, and 51.5°C, respectively. Combined with the data analysis of Table 4 and Table 5, the effects of nanofluid coolant on liquid cooling heat transfer and OHP heat transfer in hybrid BTMS show opposite effects. As graphene nanofluids enhance the thermal conductivity of coolants, in the hybrid system, the heat transfer performance of the liquid cooling plate in direct contact with the battery

surface is significantly improved, and correspondingly, the thermal load borne by the OHP is reduced. Accordingly, compared with pure water coolant, when using nanofluid coolant, the oscillation temperature and amplitude of OHP on the wall of the evaporation section are lower, indicating that the heat transfer capacity of OHP is weakened.

Figure 12 compares the T_b, T_{max}, ΔT_{max}, and the R_{BTMS} under a 280W heat load and steady-state flow conditions for the hybrid BTMS and liquid BTMS, using either water or graphene nanofluids as the coolant. Specifically, Case 1 represents the liquid BTMS using water as the coolant; Case 2 represents the hybrid BTMS using water as the coolant; Case 3 represents the liquid BTMS using graphene nanofluids as the coolant; and Case 4 represents the hybrid BTMS using graphene nanofluids as the coolant. Apart from the differences in coolant type and BTMS structure, all other conditions across the four experiments are identical.

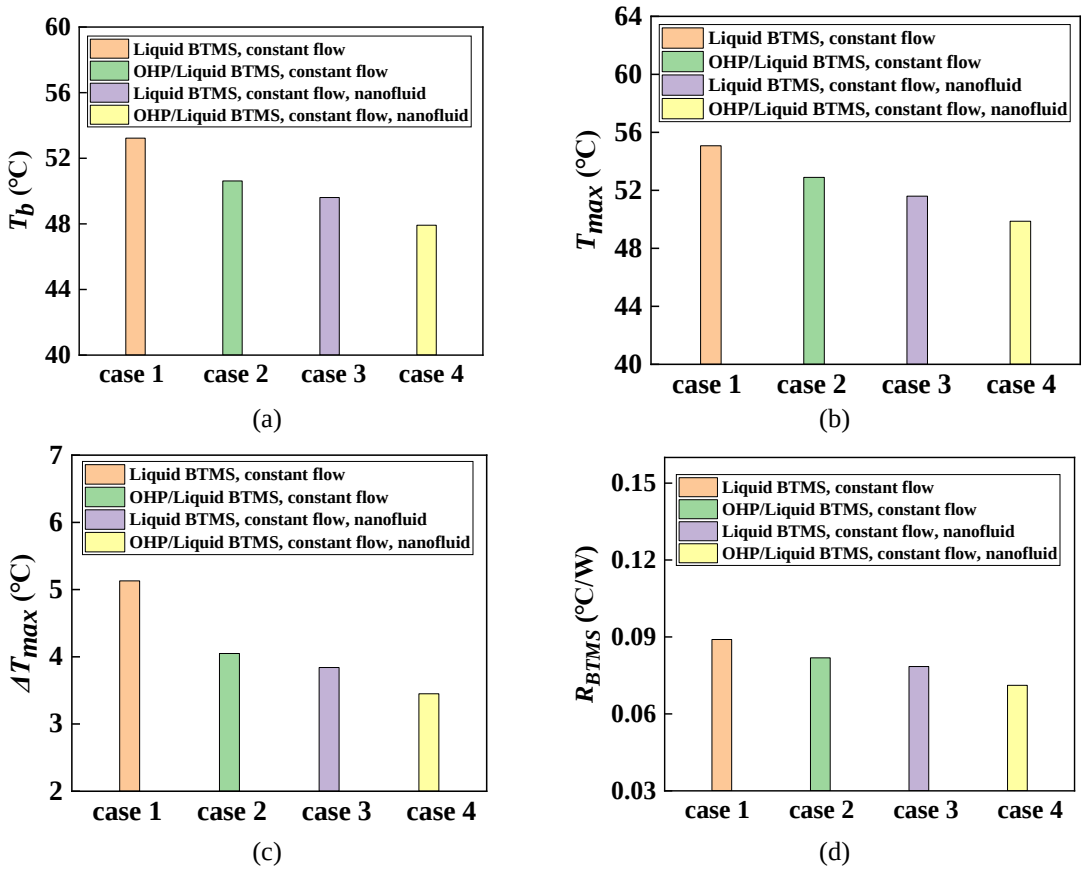

Figure 12. Heat Transfer Characteristics under different nanofluid coolant schemes: (a) T_b, (b) T_{max}, (c) ΔT_{max}, (d) R_{BTMS}

The figure clearly shows that the hybrid BTMS using nanofluid (Case 4) exhibits the best cooling performance, followed by Case 3, Case 2, and Case 1. The superior cooling performance of the hybrid BTMS with nanofluid (Case 4) can be attributed to two main factors. First, under a 280W load, the working fluid within the inverted T-shaped OHP maintains continuous oscillation, effectively utilizing the heat transfer pathway of the oscillating heat pipe in the hybrid BTMS. Second, the nanofluid significantly enhances the efficiency of liquid cooling within the system. As a result, the hybrid BTMS in Case 4 achieves optimal values for T_b, T_{max}, ΔT_{max}, and R_{BTMS}, which are 47.9°C, 49.9°C, 3.45°C, and 0.071°C/W, respectively. Compared to the liquid BTMS using water as the coolant (Case 1), both the hybrid BTMS with water (Case 2) and the liquid BTMS with graphene nanofluids (Case 3) demonstrate improved heat transfer performance. Notably, the enhancement in cooling performance provided by the 0.2% graphene nanofluids is more significant than that achieved by merely adding the inverted T-shaped OHP as an additional heat transfer path. In the hybrid BTMS, replacing pure water with nanofluid results in reductions of 2.7°C, 3.0°C, and 0.6°C in T_b, T_{max}, and ΔT_{max}, respectively.

Compared to liquid BTMS, the dual heat transfer mechanism of hybrid BTMS significantly reduces temperature variations across battery pack surfaces. Case2 achieved a 21.1% decrease in ΔT_{max} compared to Case 1, whereas Case4 showed only a 10.2% reduction in ΔT_{max} when compared to Case 3. This indicates that while the use of nanofluid coolant substantially enhances the heat transfer efficiency of liquid cooling paths in hybrid BTMS, it simultaneously weakens the forced convection effect between the OHP evaporation section and condensation section. Consequently, the heat transfer performance at the OHP end is compromised, ultimately diminishing hybrid BTMS' advantage in thermal uniformity.

4. CONCLUSIONS

Applying OHP technology to BTMS is a relatively new approach. In this study, we experimentally investigated the enhancement effect of graphene nanofluid coolant on the heat transfer performance of a liquid-cooled battery thermal management system based on an inverted T-shaped OHP (hybrid BTMS). The findings reveal that the hybrid BTMS,

which combines both liquid cooling and OHP cooling heat transfer pathways, significantly improves cooling performance and temperature uniformity compared to a standard liquid BTMS, provided that the inverted T-shaped OHP operates stably. Notably, the influence of nanofluids on heat transfer performance between the liquid cooling plate and OHP in hybrid BTMS are opposite. On the one hand, graphene nanofluid coolant can significantly improve the heat transfer efficiency of liquid cooling plate in hybrid BTMS. As the concentration of graphene nanofluid increases, the T_b decreases. On the other hand, this enhancement simultaneously weakens the forced convection effect between the evaporator and condenser sections of the OHP, resulting in reduced heat transfer performance of the OHP under low thermal load conditions. Compared to the liquid BTMS base solution, using graphene nanoparticle coolant with a 0.2% mass fraction under 280W reduced the equivalent R_{BTMS} of hybrid BTMS by 20.2%, while simultaneously lowering ΔT_{max} by 32.9%. The results show that the hybrid BTMS incorporating nanofluid coolant demonstrated superior heat dissipation and temperature uniformity performance under high thermal loads.

ACKNOWLEDGEMENTS

This work was supported by Ministry of Higher Education, Malaysia through the Fundamental Research Grant Scheme: FRGS/1/2024/TK10/UMP/02/15, Universiti Malaysia Pahang Al-Sultan Abdullah (RDU240117), and the Scientific and Technological Research Project for Education Department of Jiangxi Province in China (GJJ244911). The support for the laboratory used from Jiangxi Polytechnic University, China and Universiti Malaysia Pahang Al-Sultan Abdullah was equally acknowledged and appreciated.

CONFLICT OF INTEREST

The authors declare no conflicts of interest.

AUTHORS' CONTRIBUTION

L. Hongkun (Conceptualization; Methodology; Formal analysis; Writing - original draft; Writing - review & editing)

M. M. Noor (Supervision; Funding acquisition; Project administration; Writing - review & editing)

K. Kadirgama (Conceptualization; Resources; Writing - review & editing)

M. S. Beg (Writing - review & editing)

AVAILABILITY OF DATA AND MATERIALS

The data supporting this study's findings are available on request from the corresponding author.

ETHICS STATEMENT

This study did not involve human participants or animals. Ethical approval was therefore not required.

REFERENCES

[1] S. Rana, R. Kumar, R. S. Bharj, "Current trends, challenges, and prospects in material advances for improving the overall safety of lithium-ion battery pack," *Chemical Engineering Journal*, vol. 463, p. 142336, 2023.

[2] S. Mishra, S. Mishra, J. K. Devanuri, "Optimization of lithium-ion battery pack thermal performance: A study based on electrical, design, and discharge parameters," *Applied Thermal Engineering*, vol. 260, p. 125071, 2025.

[3] Y. Xiao, J. R. Zhao, L. Yin, B. Li, Y. Tian, "Staged thermal runaway behaviours of three typical lithium-ion batteries for hazard prevention," *Journal of Thermal Analysis and Calorimetry*, vol. 149, no. 4, pp. 1–13, 2024.

[4] P. Shrivastava, P. A. Naidu, S. Sharma, B. K. Panigrahi, A. Garg, "Review on technological advancement of lithium-ion battery state estimation methods for electric vehicle applications," *Journal of Energy Storage*, vol. 64, Art. no. 107159, 2023.

[5] M. Waseem, M. Ahmad, A. Parveen, M. Suhaib, "Battery technologies and functionality of battery management system for EVs: Current status, key challenges, and future prospects," *Journal of Power Sources*, vol. 580, p. 233349, 2023.

[6] M. Mama, M. Magui, E. Solai, T. Capurso, A. Danlos, S. Khelladi, "Comprehensive review of multi-scale lithium-ion batteries modeling: From electrochemical dynamics up to heat transfer in battery thermal management systems," *Energy Conversion and Management*, vol. 325, p. 119223, 2025.

[7] M. Manisha, S. Tiwari, R. K. Sahdev, D. Chhabra, M. Kumari, A. Ali, et al., "Advancements and challenges in battery thermal management for electric vehicles," *Renewable and Sustainable Energy Reviews*, vol. 209, p. 115089, 2025.

[8] K. Chen, Z. Zhang, B. Wu, M. Song, X. Wu, "An air-cooled system with a control strategy for efficient battery thermal management," *Applied Thermal Engineering*, vol. 236, p. 121578, 2024.

[9] D. K. Sharma, A. Prabhakar, "A review on air-cooled and air-centric hybrid thermal management techniques for Li-ion battery packs in electric vehicles," *Journal of Energy Storage*, vol. 41, p. 102885, 2021.

[10] V. Yessaulkov, A. Mitrofanov, K. Abishev, "Numerical analysis of the thermal state of a cylindrical body cooled by an internal fluid flow," *Journal of Mechanical Engineering Science*, vol. 18, no. 2, pp. 1069–1076, 2024.

[11] G. Zhao, X. Wang, M. Negnevitsky, C. Li, "An up-to-date review on the design improvement and optimization of liquid-cooling battery thermal management systems for electric vehicles," *Applied Thermal Engineering*, vol. 219, p. 119626, 2023.

[12] S. Cai, X. Zhang, J. Ji, "Recent advances in phase change materials-based battery thermal management systems for electric vehicles," *Journal of Energy Storage*, vol. 72, p. 108750, 2023.

[13] A. Khan, M. Ali, S. Yaqub, S. A. Taj, A. W. Ahmad, H. A. Khalid, et al., "Experimental investigation of passive thermal management in Li-ion battery packs using eutectic phase change materials for electric vehicles," *Journal of Power Sources*, vol. 657, p. 238108, 2025.

[14] Z. Yu, J. Zhang, W. Pan, "A review of battery thermal management systems involving heat pipes and phase change materials," *Journal of Energy Storage*, vol. 62, p. 106827, 2023.

[15] F. Zhu, Y. Wang, Y. Xie, H. Chen, Y. Zhang, "Analysis of battery thermal management systems based on flat heat pipes at high discharging rates," *Applied Thermal Engineering*, vol. 254, p. 123798, 2024.

[16] G. Zhang, Z. Liu, Z. Wu, W. Lu, Q. Yang, "Experimental investigation of a battery thermal management system based on micro heat pipe array coupled with air cooling," *Thermal Science and Engineering Progress*, vol. 60, p. 103493, 2025.

[17] H. Lu, M. M. Noor, K. Kadirgama, "Experimental study on a hybrid battery thermal management system combining oscillating heat pipes and liquid cooling," *Frontiers in Heat and Mass Transfer*, vol. 23, no. 1, pp. 299–324, 2025.

[18] A. K. Thakur, R. Sathyamurthy, R. Velraj, R. Saidur, A. K. Pandey, Z. Ma, et al., "A state-of-the-art review on advancing battery thermal management systems for fast charging," *Applied Thermal Engineering*, vol. 226, p. 120303, 2023.

[19] Y. Xu, Y. Xue, H. Qi, W. Cai, "An updated review on working fluids, operating mechanisms, and applications of pulsating heat pipes," *Renewable and Sustainable Energy Reviews*, vol. 144, Art. no. 110995, 2021.

[20] M. A. Nazari, M. H. Ahmadi, V. Blazek, L. Prokop, S. Misak, F. Atamurotov, et al., "Performance enhancement of oscillating heat pipes by structural modification: A comprehensive review," *Sustainable Energy Technologies and Assessments*, vol. 75, p. 104230, 2025.

[21] L. Hongkun, M. M. Noor, Y. Wenlin, K. Kadirgama, I. A. Badruddin, S. Kamangar, "Experimental research on heat transfer characteristics of a battery liquid-cooling system with ⊥-shaped oscillating heat pipes under pulsating flow," *International Journal of Heat and Mass Transfer*, vol. 224, p. 125363, 2024.

[22] J. Li, L. Qiao, M. Chen, D. Song, X. Zeng, "Metal oxide nanofluid-enhanced closed-loop pulsating heat pipes considering base fluid characteristics for battery thermal management in cryogenic environments," *Energy*, p. 137409, 2025.

[23] C. Diaz-Caraveo, K. Wolk, S. Miesner, M. Montemayor, A. Rodriguez, V. Kumar, et al., "Performance dry-out limits of oscillating heat pipes: A comprehensive theoretical and experimental investigation," *Journal of Thermophysics and Heat Transfer*, vol. 38, no. 1, pp. 1–11, 2024.

[24] M. Chen, J. Li, "Nanofluid-based pulsating heat pipes for thermal management of lithium-ion batteries in electric vehicles," *Journal of Energy Storage*, vol. 32, p. 101715, 2020.

[25] M. Chen, J. Li, "Experimental study on heating performance of pure electric vehicle power batteries under low-temperature environments," *International Journal of Heat and Mass Transfer*, vol. 172, p. 121191, 2021.

[26] S. Chotmanee, S. Tundee, "Experimental study on the thermal performance of oscillating heat pipes applied to lithium iron phosphate battery thermal management systems," *Journal of Research and Applications in Mechanical Engineering*, vol. 10, no. 1, pp. 1–10, 2022.

[27] W. Lv, J. Li, M. Chen, "Experimental study on thermal management performance of a power battery module using pulsating heat pipes under different strategies," *Applied Thermal Engineering*, vol. 227, p. 120402, 2023.

[28] R. Chi and S. H. Rhi, "Oscillating heat pipe cooling system for electric vehicle lithium-ion batteries with direct contact bottom cooling," *Energies*, vol. 12, no. 9, p. 1698, 2019.

[29] Z. Chi, Z. Guo, X. Gong, "Startup and heat transfer characteristics of L-shaped pulsating heat pipes," *Journal of Refrigeration*, vol. 43, pp. 99–105, 2022.

[30] W. S. Chung, J. S. Lee, S. H. Rhi, "Thermal management system using pulsating heat pipes for cylindrical battery cells," *Journal of Mechanical Science and Technology*, vol. 37, no. 6, pp. 1–15, 2023.

[31] L. Cattani, M. Malavasi, F. Bozzoli, V. D'Alessandro, L. Giammichele, "Two-phase cooling system for electric vehicle batteries based on a 3D pulsating heat pipe," *Energies*, vol. 17, p. 3236, 2024.

[32] L. Hongkun, M. M. Noor, K. Kadirgama, M. S. Beg, "Startup, heat transfer, and flow characteristics of a ⊥-shaped oscillating heat pipe for hybrid battery thermal management applications," *Applied Thermal Engineering*, vol. 269, Art. no. 125984, 2025.

[33] M. A. Nazari, M. H. Ahmadi, R. Ghasempour, M. B. Shafii, "Improving thermal performance of pulsating heat pipes: A review on working fluids," *Renewable and Sustainable Energy Reviews*, vol. 91, pp. 630–638, 2018.

[34] C. Xu, S. Xu, S. Wei, P. Chen, "Experimental investigation of heat transfer in pulsating flow of graphene oxide–water nanofluids in microchannels," *International Communications in Heat and Mass Transfer*, vol. 110, p. 104403, 2020.

[35] J. Chen, B. Yao, C. Li, G. Shi, "An improved Hummers method for eco-friendly synthesis of graphene oxide," *Carbon*, vol. 64, pp. 225–229, 2013.

[36] V. Vijayakanth, K. Chintagumpala, "Review on the effect of dispersant type and medium viscosity on magnetic hyperthermia of nanoparticles," *Polymer Bulletin*, vol. 80, pp. 4737–4781, 2023.

[37] F. M. Hanapiah, I. A. Zakaria, S. R. Makhsin, N. Hamzan, "Behaviour of ternary hybrid nanofluids comprising graphene oxide, aluminium oxide, and silicon dioxide on heat transfer rates," *Journal of Mechanical Engineering Science*, vol. 18, no. 2, pp. 9988–10003, 2024.

[38] A. Arshad, M. Jabbal, Y. Yan, D. Reay, "A review on graphene-based nanofluids: Preparation, characterization, and applications," *Journal of Molecular Liquids*, vol. 279, pp. 444–484, 2019.

[39] S. Ghosh, S. Subudhi, "Developments in fuel cells and electrochemical batteries using nanoparticles and nanofluids," *Energy Storage*, vol. 4, no. 3, p. e288, 2022.